Theoretical Kinetic Studies of Models for Binding Myosin Subfragment-1 to Regulated Actin: Hill Model versus Geeves Model

Yi-der Chen,* Bo Yan,* Joseph M. Chalovich,† and Bernhard Brenner‡

*Mathematical Research Branch, National Institute of Diabetes and Digestive and Kidney Diseases, National Institutes of Health, 9190 Rockville Pike, Bethesda, Maryland 20892-2690, †Department of Biochemistry, East Carolina University Medical School, Greenville, North Carolina 27858-4354 USA and ‡Department of Molecular and Cell Physiology, Medical School Hannover, D-30623 Hannover, Germany

ABSTRACT It was previously shown that a one-dimensional Ising model could successfully simulate the equilibrium binding of myosin S1 to regulated actin filaments (T. L. Hill, E. Eisenberg and L. Greene, *Proc. Natl. Acad. Sci. U.S.A.* 77:3186–3190, 1980). However, the time course of myosin S1 binding to regulated actin was thought to be incompatible with this model, and a three-state model was subsequently developed (D. F. McKillop and M. A. Geeves, *Biophys. J.* 65:693–701, 1993). A quantitative analysis of the predicted time course of myosin S1 binding to regulated actin, however, was never done for either model. Here we present the procedure for the theoretical evaluation of the time course of myosin S1 binding for both models and then show that 1) the Hill model can predict the "lag" in the binding of myosin S1 to regulated actin that is observed in the absence of Ca^{++} when S1 is in excess of actin, and 2) both models generate very similar families of binding curves when [S1]/[actin] is varied. This result shows that, just based on the equilibrium and pre-steady-state kinetic binding data alone, it is not possible to differentiate between the two models. Thus, the model of Hill et al. cannot be ruled out on the basis of existing pre-steady-state and equilibrium binding data. Physical mechanisms underlying the generation of the lag in the Hill model are discussed.

INTRODUCTION

Muscle contraction involves cyclic binding and unbinding of myosin heads (cross-bridges) of the thick filament to actin of the thin filament driven by the hydrolysis of ATP. Tropomyosin (Tm) and troponin (Tn) are proteins responsible for the Ca^{++} regulation of the interaction between myosin and actin in vertebrate skeletal muscle. In solution, myosin and its subfragment 1 (S1) bind to unregulated filamentous actin (F-actin in the absence of Tm and Tn) with no measurable cooperativity, and the binding kinetics may involve at least two binding steps (Trybus and Taylor, 1980; Geeves and Halsall, 1987). In the presence of Tm and Tn, the equilibrium binding is highly cooperative in the absence of Ca^{++} and is slightly cooperative in the presence of Ca^{++} (Greene and Eisenberg, 1980). The cooperative binding isotherm at equilibrium was first interpreted with a one-dimensional Ising model by Hill et al. (1980) (referred to as the Hill model from now on). In this model (see Fig. 1), a single Tm–Tn and seven actin monomers form a unit that can exist in two states, state 1 (inactivated) and state 2 (activated), with higher binding affinities for Ca^{++} and myosin (or S1) for the latter. Thus, the binding of Ca^{++} and myosin to the actin modulates the distribution between the two states of each unit in the thin filament. The binding of myosin is cooperative because seven actin monomers in a unit change state as a group and because of the existence of interactions between two neighboring units. Because equilibrium binding was the only concern, the kinetics of the binding reactions was not specified in the model. The Hill model, however, was not only shown to account for equilibrium binding data but also for the steady-state kinetic patterns of ATP hydrolysis at both high and low free Ca^{++} and for both excess S1 and excess actin (Hill et al., 1981). This model also incorporated the different effect of troponin–tropomyosin on the binding of different nucleotide complexes of S1 (Chalovich et al., 1981).

The cooperative S1 binding was reinterpreted by Geeves and his colleagues in terms of a two-state model at first (Geeves and Halsall, 1987; McKillop and Geeves, 1991) and then a three-state model (McKillop and Geeves, 1993) (referred to as the Geeves model from now on), in which the S1 binding kinetics are strictly coupled to the two-step mechanism of S1 binding to F-actin in the absence of Tm and Tn. In this three-state model (see Figs. 2 and 3), seven actin monomers and a Tm–Tn molecule also form a unit. Each unit in the thin filament can exist in three states with different S1 binding properties: the "blocked" state where S1 binding is completely prohibited, the "closed" state where only the first step of the two-step binding mechanism can take place, and the "open" state where both steps are in operation. In this model, the equilibrium association constant and the kinetic rate constants of binding of S1 to actin monomers in the three states are independent of the presence of Ca^{++}. Ca^{++} affects only the distribution between the blocked and the closed states and therefore the availability of S1 binding sites on the actin filament. In addition, this model does not consider explicitly the nearest-neighbor interaction between cooperative units.

Received for publication 10 November 2000 and in final form 26 February 2001.

Address reprint requests to Yi-der Chen at the Mathematical Research Branch, NIDDK, NIH, 9190 Rockville Pike, Bethesda, MD 20892-2690. Tel.: 301-496-5436; Fax: 301-402-0535; E-mail: ydchen@helix.nih.gov.

0006-3495/01/05/2338/12 $2.00

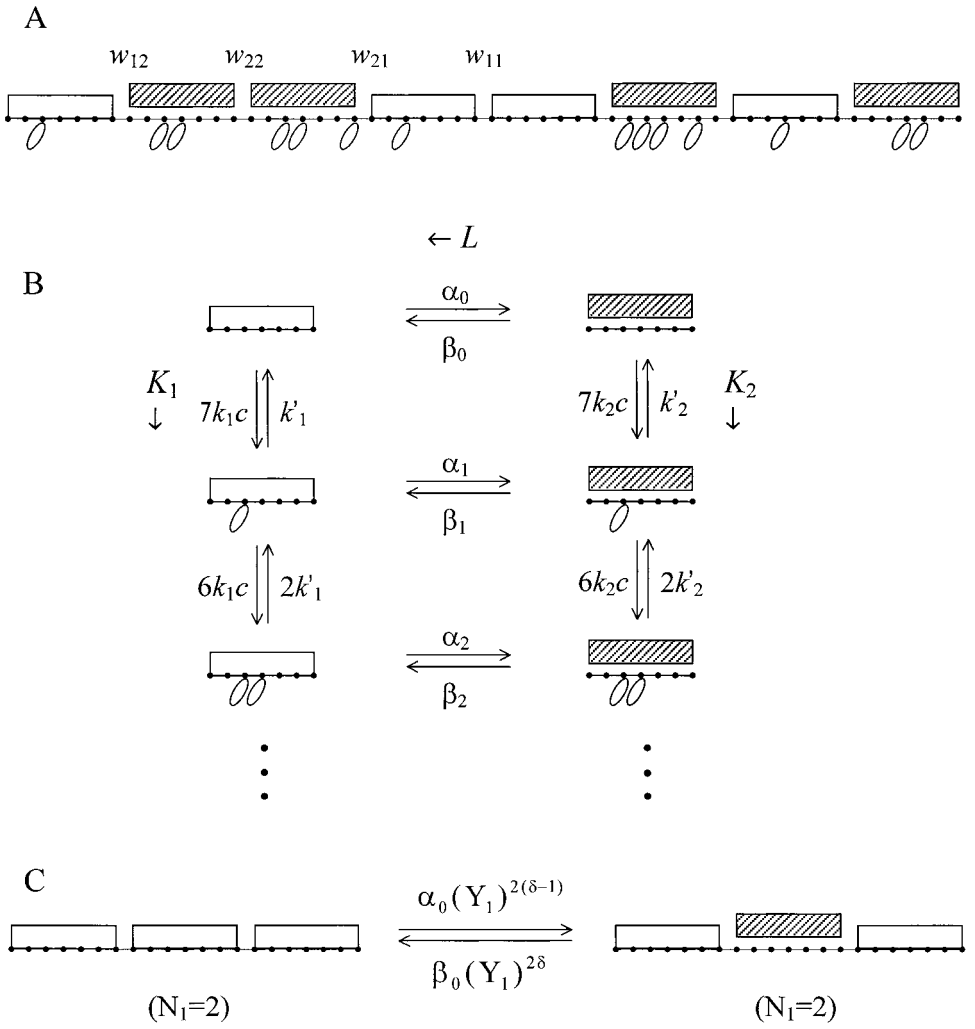

FIGURE 1 Schematic representation of the two-state Hill model. (*A*) The configuration of a regulated actin filament. A unit is composed of one Tm–Tn complex plus seven actin sites. Each unit can exist in either state 1 (*blank rectangle*, the inactive state) or state 2 (*shaded rectangle*, the active state). The w_{ij} represent the nearest-neighbor interactions between two neighboring units in states *i* and *j*. (*B*) The kinetic diagram showing all the transitions for an isolated Tm–Tn–actin unit. *c* is the concentration of free S1 in solution and the k_i are the intrinsic binding and unbinding rate constants of S1 to an isolated actin monomer. The rate constants are related to the equilibrium constants as $L = \alpha_0/\beta_0$, $K_1 = k_1/k'_1$, $K_2 = k_2/k'_2$. (*C*). Effect of cooperativity on the transitions of a unit between inactive and active states. N_1 is the number of the two neighbors that are in state 1, δ is a fixed constant between 0 and 1, and $Y_1 \equiv Y_{11}/Y_{12} \equiv \exp(-(w_{11} - w_{12})/k_BT)$.

Recently, the molecular structure of regulated actin filaments has been studied using electron microscopy and three-dimensional image reconstruction (Vibert et al., 1997; Xu et al., 1999). It has been shown that addition of Ca^{++} causes an ~25° azimuthal movement of tropomyosin from the outer to inner domain of actin and that S1 binding causes a further 10° shift, resulting in complete exposure of the myosin binding site on actin. That is, structurally the actin filament can be considered to exist in three states: the fully-off, the intermediate calcium, and the fully-on state (Tobacman and Butters, 2000). It is easy to assume that the Geeves model is more consistent with this structural information, because it also contains three kinetic states. However, the Hill model is also consistent with this three-state structural model because the Hill model has enough substates to predict different levels of ATPase activity for the conditions used to obtain three structures of the actin filament (Hill et al., 1981). At low saturation with myosin and in the absence of Ca^{++}, the actin units are in state $1_{(0)}$ where the subscript (0) means that the actin unit has no bound Ca^{++}. At low bound S1 and in the presence of saturating Ca^{++}, the rate is increased ~80-fold (28-fold increase in k_{cat} and decrease in the K_M to 0.3 of the original value; Chalovich and Eisenberg, 1982). At this condition, actin filaments are in state $1_{(2)}$ of the Hill model (the actin filament is in the same major state 1, but it is in a different sub-state with two bound Ca^{++} ions per troponin). Finally, at high saturation with myosin and with bound Ca^{++}, the actin filament is in state $2_{(2)}$ and the rate increases another eight-fold (two-fold increase in k_{cat} and a decrease in the K_M to 0.25; Williams et al., 1988). It is thought that the ability of actin to stimulate the ATPase activity of myosin is about the same if actin is in state $2_{(0)}$ (no bound Ca^{++}) and in state $2_{(2)}$ (two bound Ca^{++}). Thus, there are sufficient chemical states in both the Hill model and the Geeves model to account for the observed structural states. A major difference between the two models is that the intermediate structural state is assumed to be required in the absence of Ca^{++} in the Geeves model, but not in the Hill model.

As far as fitting the equilibrium binding isotherms for S1 to actin is concerned, the Hill and Geeves models are mathematically equivalent. However, the molecular kinetic

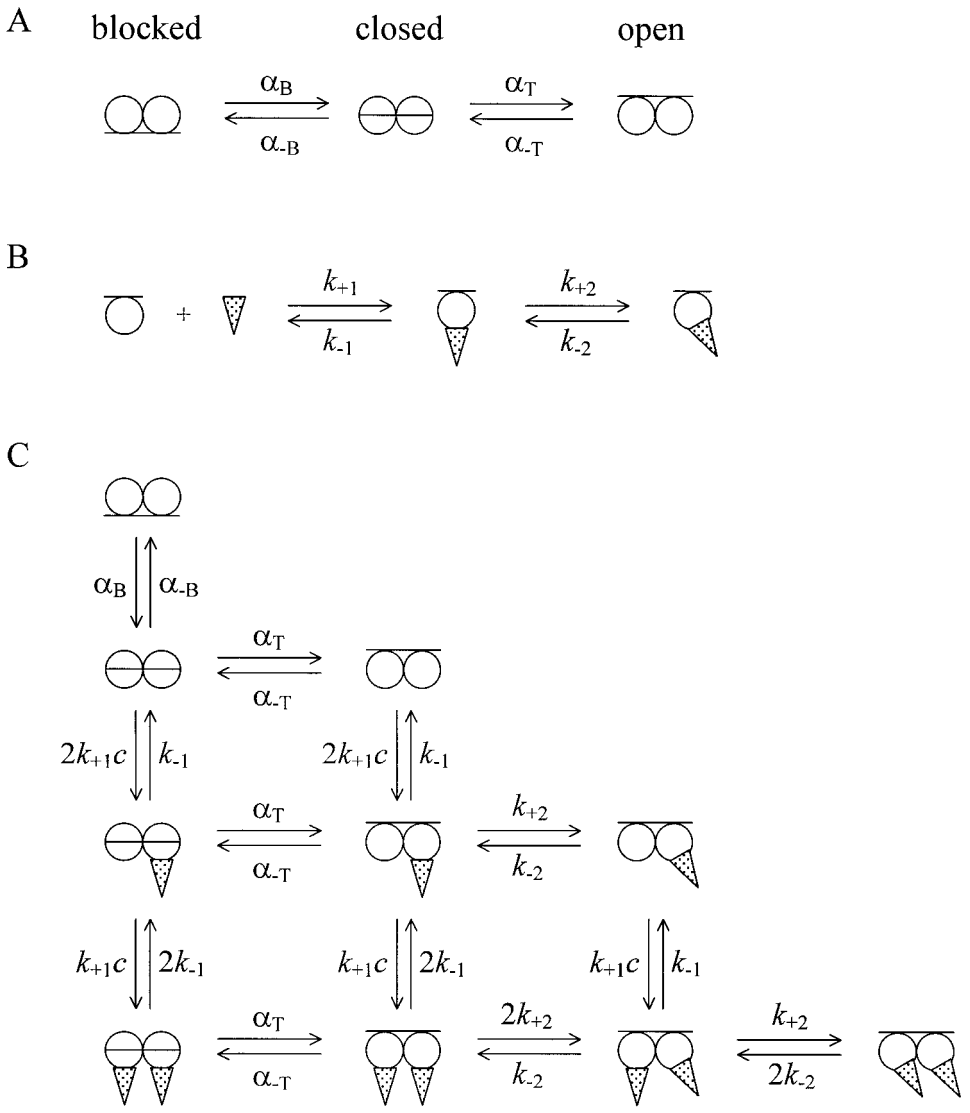

FIGURE 2 Schematic representation of the three-state Geeves model for the special case that each Tm–Tn complex is assumed to cover two actin-sites only. (*A*) The kinetic diagram of a Tm–Tn–actin unit in the absence of S1. (*B*) The two-step mechanism for the binding of S1 to an actin site in the open state. The same mechanism operates in the binding of S1 to pure F-actin in the absence of Tm–Tn. (*C*) The complete kinetic diagram for the binding of S1 to a Tm–Tn unit for the special two-actin case. The diagram can be extended to cases with an arbitrary number of actin monomers as shown in Fig. 3 for the seven-monomer case.

mechanisms of activation and myosin binding of the two models are fundamentally different. For example, in the Geeves model the rate constant of binding of S1 to actin monomers in a regulated actin filament is independent of whether the troponin of the unit is bound with Ca^{++} or not, but this is not true for the Hill model. Also, the two-step mechanism of S1 to actin is not mandatory in the Hill model although two-step binding may be included. In addition, the cooperativity is handled differently in the two models. Finally and most importantly, unlike in the Geeves model, an isolated actin unit can jump directly from the "off" state to the "on" state without going through an intermediate state in the Hill model.

Recently, the pre-steady-state kinetics of S1 binding to regulated actin filaments in the absence and presence of Ca^{++} have been studied in several laboratories by measuring light scattering and fluorescence changes in pyrene-labeled actin (Trybus and Taylor, 1980; McKillop and Geeves, 1993). It has been found that, when actin is in excess of S1, the time course of the fluorescence change or the light scattering can be described by a single exponential function in both the presence and absence of calcium. In contrast, when S1 is in excess of actin, a single-exponential is observed in the presence but not in the absence of Ca^{++}. In the absence of Ca^{++}, the shape of the time course of myosin S1 binding to regulated actin is sigmoidal (referred to as having a "lag"). It was assumed that the two-state kinetic mechanism of the Hill model would not be able to generate this kind of lag in the time course of S1 binding. Quantitatively, it was also argued that the Hill model did not have enough actin in the on state before S1 mixing to account for the fast S1 binding rate measured at early times (Trybus and Taylor, 1980). The three-state Geeves model was assumed to be able to solve all these problems (McKillop and Geeves, 1993). However, a quantitative analysis of the entire time course of S1 binding to regulated actin predicted by the two models has never been carried out; the properties of the models have only been discussed qualita-

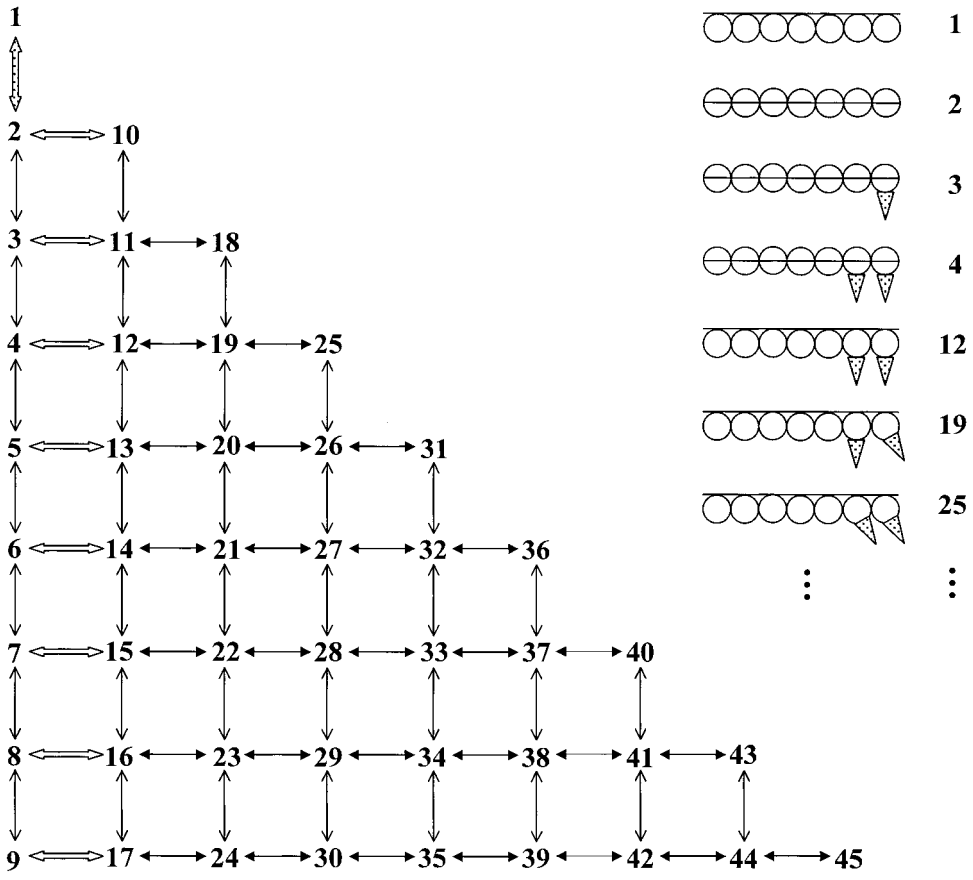

FIGURE 3 The complete kinetic diagram of the Geeves model for the binding of S1 to a Tm–Tn unit with seven actin monomers. The configurations of some states are shown at the upper right corner. The dotted block arrow represents the transition from the blocked to the closed state and the blank block arrow represents the transition from the closed to the open state. Arrows with barbed ends and those with triangle ends represent, respectively, the first and the second steps of the two-step S1 binding reactions.

tively based on the apparent rate constants obtained by fitting the time courses with a one-exponential function (McKillop and Geeves, 1993). Thus, it is not clear whether the Hill model is really unable to generate the observed lag and the fast initial rate in the kinetic curves of S1 binding. Nor has it been clearly demonstrated that the Geeves model is really able to predict the characteristic family of time courses of S1 binding for different S1 and actin concentrations.

In this paper, the kinetic properties of the two models are studied theoretically with the aim to address the questions mentioned above. We first discuss the mathematical procedures for the calculation of time course for S1 binding and then discuss the predictions of the two models. Due to the explicit inclusion of cooperativity in the model, the kinetics of S1 binding in the Hill model has to be evaluated using the Monte Carlo simulation method. In contrast, the kinetic binding curves of the Geeves model can be calculated numerically. We show that both models are equivalent in predicting the kinetics of S1 binding to regulated actin. Specifically, we show that, in contrast to what was suggested in the past, the Hill model is just as well able to generate the lag in the time course of S1 binding to regulated actin when excess S1 is mixed with actin in the absence of calcium. This shows that it is not possible to differentiate the two models based on equilibrium and pre-steady-state kinetic data of S1 binding alone. This result also implies that, in the absence of Ca^{++}, the activation of actin filament from the off to the on state does not require the existence of an intermediate state as in the Geeves model. The mechanisms underlying the generation of the lag in the S1 binding kinetic curves in the two-state model of Hill are discussed.

We have not attempted to evaluate all possible models of regulation but have focused on the original Hill model and the Geeves three-state model with the intent of understanding those factors responsible for the complex binding and kinetics of the regulated actomyosin system. Several other theoretical treatments of regulation have been published such as the elaborate models of Zou and Phillips (1994) and Tobacman and Butters (2000).

MODEL AND MATHEMATICAL ANALYSIS

The Hill model

The basic equilibrium and kinetic features of the Hill model are described schematically in Fig. 1. A regulated actin filament is composed of a linear array of units, each of them contains a Tm–Tn complex and 7 actin monomers. Each unit can exist in two states, state 1 (the inactive, or off, state) and state 2 (the active, or on, state), with different Ca^{++} and S1 affinities. Let w_{ij} ($i, j = 1, 2$) denote the interaction energies between two neighboring units in states i and j, respectively, as shown in Fig. 1 *A*. And, as shown in Fig. 1 *B*, let K_1 and K_2 denote the equilibrium constants of

binding S1 to an actin monomer in states 1 and 2, respectively, and L be the intrinsic equilibrium constant for the transition from state 2 to state 1 of an isolated Tm–Tn–actin unit with no bound S1. Then, as shown by Hill et al. (1980), the fraction of the total actin monomers bound with S1 (θ) in this model can be expressed as a function of the concentration (c) of the free S1 in solution as

$$\theta = p_1 \frac{K_1 c}{1 + K_1 c} + p_2 \frac{K_2 c}{1 + K_2 c}, \tag{1}$$

where

$$p_1 = \frac{2aY^{-1}}{\sqrt{(a - 1 + \sqrt)}}, p_2 = \frac{2aY^{-1}}{\sqrt{(1 - a + \sqrt)}}, \tag{2}$$

$$\sqrt = [(1 - a)^2 + 4aY^{-1}]^{1/2}, \tag{3}$$

$$a = (1 + K_2 c)^7 / L'(1 + K_1 c)^7, \tag{4}$$

$$Y \equiv Y_{11} Y_{22} / Y_{12}^2, \tag{5}$$

$$L' \equiv L Y_{11} / Y_{22}, \tag{6}$$

and Y_{ij} ($\equiv \exp(-w_{ij}/k_B T)$, where w_{ij} is the interaction energy between two neighboring units in states i and j, and $k_B T$ is the product of the Boltzmann constant and the temperature) is the cooperativity factor. For simplicity, we have assumed that $Y_{12} = Y_{21}$. Eq. 1 can thus be used to evaluate the values of K_1, K_2, L', and Y from the experimental binding isotherm.

One must note that Eq. 1 defines the fraction of the total actin monomers bound with S1. Thus, Eq. 1 can be used directly for data analysis when the measured quantity reflects the total amount of S1 bound to actin (such as when measuring the light scattering). Recently, the fluorescence of pyrene attached to actin monomers has been shown to monitor the amount of actin monomers in state 2 that are bound with S1. In this case, the fractional change of the pyrene fluorescence in the system, $R(c)$, is related to the second term of Eq. 1 as

$$R(c) \equiv \frac{F(c) - F(0)}{F(\infty) - F(0)} = p_2 \frac{K_2 c}{1 + K_2 c}, \tag{7}$$

where $F(c)$ represents the total pyrene fluorescence of the system when the free S1 concentration in the system is c.

Due to the existence of cooperativity, the kinetic curves of S1 binding to actin filaments have to be evaluated by Monte Carlo simulation. The basic rate constants describing the kinetics of S1 binding and conformational transitions of an isolated Tm–Tn–actin unit are shown in Fig. 1 *B*. They are the S1 binding and dissociation rate constants, k_1, k_1', k_2 and k_2', and the transition rate constants of an isolated Tm–Tn–actin unit between active (state 2) and inactive (state 1) states, α_m and β_m ($m = 0, 1, 2, \ldots, 7$) where m refers to the number of S1 bound to the unit. These rate constants are not independent of each other, but related to the equilibrium constants,

$$k_1/k_1' = K_1, \quad k_2/k_2' = K_2, \tag{8}$$

$$\beta_0/\alpha_0 = L, \tag{9}$$

$$\beta_m/\alpha_m = L(K_1/K_2)^m, \quad m = 1, 2, \ldots, 7. \tag{10}$$

Because K_1 and K_2 can be obtained from the equilibrium-binding isotherm, only one rate constant in each of the two equations in Eq. 8 can be chosen as the independent parameter. As shown in Eqs. 5 and 6, the value of L is not determined even when the values of Y and L' are known (from the binding isotherm). Therefore, both α_0 and β_0 are treated as independent rate parameters. In general, with a given L (when the values of α_0 and β_0 are assigned) there are infinite ways to assign the values of individual α_m and β_m that are consistent with Eq. 10, depending on how the factor $(K_1/K_2)^m$ is partitioned between the two rate constants. For simplicity, let us assume that they can be expressed as

$$\alpha_m = \alpha_0 (K_1/K_2)^{m(\gamma-1)}, \tag{11}$$

$$\beta_m = \beta_0 (K_1/K_2)^{m\gamma}, \tag{12}$$

where γ is a parameter with values between 0 and 1. Note that Eqs. 11 and 12 are also applicable to the $m = 0$ case and therefore are the general rate expressions for the transitions between states 1 and 2 of a Tm–Tn–actin unit.

The kinetic parameters discussed above are for isolated Tm–Tn–actin units only. In a filament, the transition rate constants, α_m and β_m ($m = 0, 1, \ldots, 7$), are influenced by the cooperativity of the system. Let $\bar{\alpha}_m$ and $\bar{\beta}_m$ represent the cooperativity-affected rate constants. Then, as shown in Appendix A, they can be expressed as

$$\bar{\alpha}_m = \alpha_m (Y_1 Y_2)^{N_1(\delta-1)} (Y_2)^{2(1-\delta)}, \tag{13}$$

$$\bar{\beta}_m = \beta_m (Y_1 Y_2)^{N_1 \delta} (Y_2)^{-2\delta}, \tag{14}$$

where δ is a constant valued between 0 and 1, $Y_1 \equiv Y_{11}/Y_{12}$, $Y_2 \equiv Y_{22}/Y_{12}$, and N_1 is the number of the two neighboring units that are in state 1. Note that N_1 can have values of 0, 1, or 2 only (see Fig. 1 *C*) and that the values of Y_1 and Y_2 can be evaluated from Eqs. 5 and 6 when the values of Y and L' are determined from equilibrium binding isotherm and the value of L is given by the assigned α_0 and β_0. In fitting the model to any given kinetic curve, k_1', k_2', α_0, β_0, γ, and δ are chosen as the independent parameters.

To evaluate the kinetics of S1 binding using the Monte Carlo method, we follow the transitions of a single actin filament among its various states on a computer as a function of time and obtain the ensemble-averaged time course by repeating the process for a large number of times (Chen and Hill, 1983; Chalovich et al., 1995). That is, we treat the actual system as an ensemble of identical and independent small systems, each containing only one actin filament with a small volume. The kinetics of the actual system is then represented by the ensemble average of the kinetics of a single small system. During the simulation, the concentration of free S1 in solution changes as a function of time. Let c_{S1}^0 and c_A^0 be the total concentrations of S1 and actin monomers, respectively. Then the concentration of free S1 within each small system can be expressed as $c = c_{S1}^0 - (n/M)c_A^0$ where n is the number of bound S1 on an actin filament and M is the total number of actin monomers in an actin filament ($M = 700$ in all calculations).

The program to simulate the experimental S1 binding process consists of two parts. At first, the system is simulated in the absence of S1 until the system is at equilibrium. Then S1 is added to the system and the kinetic simulation starts. Histograms of bound S1 in the two states are obtained as a function of time after S1 addition. The process is repeated a thousand times and the kinetic curve of S1 binding is obtained from the average of these histograms. In this study, the number of actin monomers in an actin filament is fixed at 700. Doubling the number to 1400 was found to cause very little change in the simulated results.

The Geeves model

As in the Hill model, a regulated actin filament is also composed of Tm–Tn–actin units. Each unit contains seven actin monomers and can exist in three states: blocked, closed, and open (see Fig. 2 *A*). A unit is unable to bind S1 if the unit is in the blocked state; S1 can only bind to the closed and open states. The binding of S1 to actin involves a two-step mechanism with the second step occurring only when the unit is in the open state (see Fig. 2 *B*). In contrast to the Hill model, there is no cooperativity between neighboring units. Therefore, each unit can be treated independently. The diagram describing the kinetic mechanism of the model is shown in Fig.

2 *C* for the case with two actin monomers in each unit. The kinetic diagram for the seven-actin case without showing the rate constants is shown in Fig. 3. There are a total of 45 states in this case. The differential equations describing the kinetic behavior of the system in Fig. 3 can be solved numerically as will be shown below.

Let K_1^G and K_2^G be the equilibrium constants of the two-step S1 binding reactions to actin and K_B and K_T be the equilibrium constant between the blocked and the closed and between the closed and the open states, respectively. Then the fraction of total actin monomers bound with S1 can be expressed as (McKillop and Geeves, 1993)

$$\theta = \frac{K_1^G c[K_T(1 + K_2^G)P^6 + Q^6]}{K_T P^7 + Q^7 + 1/K_B}, \tag{15}$$

where $P \equiv 1 + K_1^G c(1 + K_2^G)$, $Q \equiv 1 + K_1^G c$, and c is the concentration of the free S1 in solution. In contrast, if one is measuring the fluorescence of pyrene attached to actin, then the fractional change in fluorescence is related to these constants as

$$R(c) = \frac{K_1^G c P^6[K_T(1 + K_2^G)^7 + 1]}{(K_T P^7 + Q^7 + 1/K_B)(1 + K_2^G)^6}. \tag{16}$$

Eqs. 15 and 16 can be used to evaluate the equilibrium constants, K_1^G, K_2^G, K_B, and K_T, using the binding isotherm.

As shown in Fig. 2 *C*, there are eight basic rate constants for the Geeves model: α_B, α_{-B}, α_T, α_{-T}, k_{+1}, k_{-1}, k_{+2}, and k_{-2}. However, they are related to the equilibrium constants as: $K_B = \alpha_B/\alpha_{-B}$, $K_T = \alpha_T/\alpha_{-T}$, $K_1^G = k_{+1}/k_{-1}$, $K_2^G = k_{+2}/k_{-2}$. Thus, only four rate constants are independent.

With the kinetic diagram given in Fig. 3, the differential equations describing the kinetic behavior of the probability, $p_i(t)$, for each state in the diagram can be written down immediately. For example,

$$\frac{dp_1(t)}{dt} = -\alpha_B p_1 + \alpha_{-B} p_2, \tag{17}$$

$$\frac{dp_2(t)}{dt} = \alpha_B p_1 - (\alpha_{-B} + 7k_{+1}c + \alpha_T)p_2 + k_{-1}p_3 + \alpha_{-T}p_{10}, \tag{18}$$

$$\vdots$$

$$\frac{dp_{45}(t)}{dt} = k_{+2}p_{44} - 7k_{-2}p_{45}, \tag{19}$$

where α_B, k_{+1}, etc. are the rate constants shown in Fig. 2. The value of c at any given time is related to the total concentration of S1, c_{S1}^0, as

$$c = c_{S1}^0 - (c_A^0/7)(\Lambda_3 + 2\Lambda_4 + 3\Lambda_5 + 4\Lambda_6 + 5\Lambda_7 + 6\Lambda_8 + 7\Lambda_9), \tag{20}$$

where c_A^0 is the total concentration of actin monomers in the system, and Λ_i represents the sum of all the ps on the ith row in Fig. 3,

$$\Lambda_3 = p_3 + p_{11} + p_{18}, \tag{21}$$

$$\Lambda_4 = p_4 + p_{12} + p_{19} + p_{25}, \tag{22}$$

etc.

At t = 0, all units are at equilibrium and free of bound S1. Thus, it is easy to show that the only states in Fig. 3 with non-zero probabilities are states 1, 2, and 10:

$$p_1(0) = 1/\Sigma, \tag{23}$$

$$p_2(0) = K_B/\Sigma, \tag{24}$$

$$p_{10}(0) = K_B K_T/\Sigma, \tag{25}$$

where

$$\Sigma \equiv 1 + K_B(1 + K_T). \tag{26}$$

Eqs. 17–19 can be solved numerically with the initial probabilities given in Eqs. 23–25 at given c_{S1}^0 and c_A^0.

After the $p_i(t)$ are obtained, the time-dependent fractional saturation of the total actin sites $\theta(t)$ can be evaluated as

$$\theta(t) = \tfrac{1}{7}(\Lambda_3 + 2\Lambda_4 + 3\Lambda_5 + 4\Lambda_6 + 5\Lambda_7 + 6\Lambda_8 + 7\Lambda_9), \tag{27}$$

where Λ_i is defined before in Eqs. 21, 22, etc. The fractional saturation of the pyrene fluorescence change $R(t)$ can be evaluated as

$$R(t) = \tfrac{1}{7}(\Omega_3 + 2\Omega_4 + 3\Omega_5 + 4\Omega_6 + 5\Omega_7 + 6\Omega_8 + 7\Omega_9), \tag{28}$$

where Ω_i denotes the sum of all the p_i on the i column in Fig. 3: $\Omega_9 = p_{45}$, $\Omega_8 = p_{43} + p_{44}$, etc.

MODEL CALCULATIONS

The main purpose of this paper is to examine whether the Hill model can reproduce the same time course of S1 binding to actin as predicted by the Geeves model. Specifically, we wanted to examine whether both models can account for the lag observed experimentally by McKillop and Geeves (1993) when mixing excess S1 to regulated actin in the absence of Ca^{++}. Thus, in this study, we first determined the set of kinetic parameters necessary for the Geeves model to reproduce the binding curves in Fig. 4 *A* of McKillop and Geeves (1993). Additional binding curves at different S1/actin ratios for the Geeves model were then calculated using these parameters and the question of whether the two models are kinetically equivalent was examined by fitting the Hill model to these binding curves.

Binding curves generated by the Geeves model

As discussed before, there are four kinetic reactions in the Geeves model: transitions between the blocked and the closed states and between the closed and the open state of the actin units and the two reactions of the two-step S1 binding. Two general rules must be obeyed when choosing the rate constants for model fitting. First, the ratio of the forward and the backward transition rate constants of any reaction must obey the equilibrium constants listed in Table 1 of McKillop and Geeves (1993). Therefore, there are only four independent rate constants to be found for the model. Second, the rate constants of the two-step S1 binding, k_{+1}, k_{-1}, k_{+2}, and k_{-2}, remain the same in the presence and in the absence of Ca^{++} (McKillop and Geeves, 1993).

The kinetic parameters obtained necessary for the Geeves model to fit the curves in Fig. 4 *A* of McKillop and Geeves (1993) are listed in Table 1. A family of time courses of S1 binding to actin that differed in the concentration of S1 and actin are shown in Fig. 4 in dashed curves. At all concentrations of actin and S1, the Geeves model predicts that the observed rate of binding of S1 to actin is faster in the presence of Ca^{++}. In the cases where [S1] ≥ [actin], the model predicts a lag in the binding in the absence of Ca^{++} (Fig. 4, *A* and *B*). There is, however, little or no lag in the presence of Ca^{++} or when [actin] > [S1] (Fig. 4 *C*).

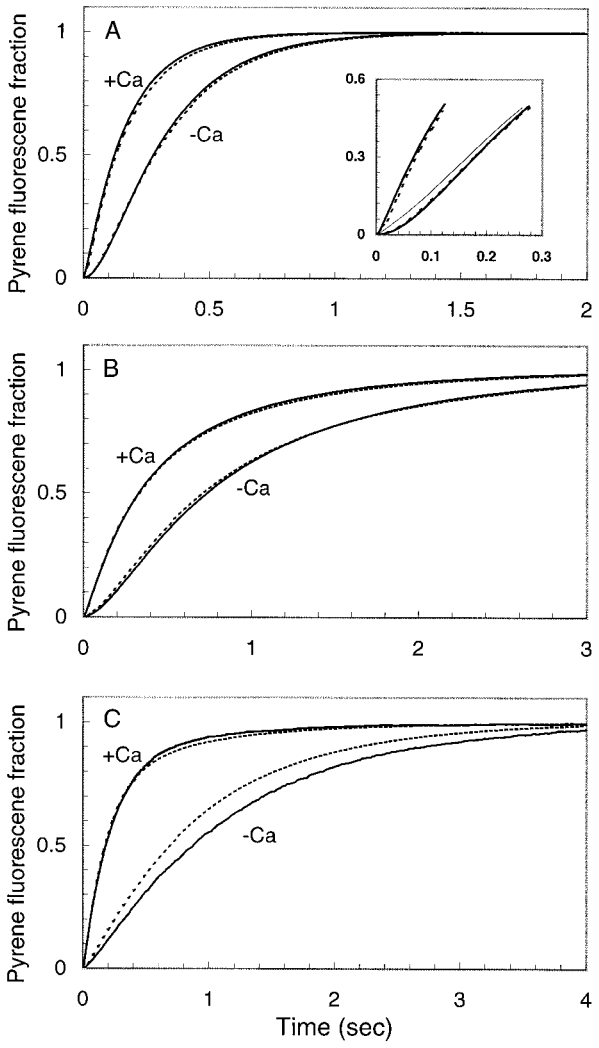

FIGURE 4 Calculated fractional pyrene-fluorescence kinetic curves using the kinetic parameters in Tables 3 and 1 for the Hill (*solid lines*) and the Geeves (*dashed lines*) models, respectively. Three different concentrations of S1 and actin were used in these models and a single exponential model was fitted to the exponential part of each curve for comparison. (*A*) [S1] = 2.5 μM, [Actin] = 0.5 μM. Geeves model: $k_{obs}(+Ca^{++})$ = 5.8 s^{-1}, $k_{obs}(-Ca^{++})$ = 3.6 s^{-1}. Hill model: $k_{obs}(+Ca^{++})$ = 6.0 s^{-1}, $k_{obs}(-Ca^{++})$ = 3.8 s^{-1}. For the absence of Ca^{++} cases, the curves after 0.2 s were fitted. (*B*) [S1] = 1 μM, [Actin] = 1 μM. Geeves model: $k_{obs}(+Ca^{++})$ = 2.0 s^{-1}, $k_{obs}(-Ca^{++})$ = 1.1 s^{-1}. Hill model: $k_{obs}(+Ca^{++})$ = 1.9 s^{-1}, $k_{obs}(-Ca^{++})$ = 1.1 s^{-1}. The curves after 0.1 s were fitted with Ca^{++} absent. (*C*) [S1] = 0.25 μM, [Actin] = 2.5 μM. Geeves model: $k_{obs}(+Ca^{++})$ = 3.9 s^{-1}, $k_{obs}(-Ca^{++})$ = 1.0 s^{-1}. Hill model: $k_{obs}(+Ca^{++})$ = 3.5 s^{-1}, $k_{obs}(-Ca^{++})$ = 0.85 s^{-1}. Inset in (*A*), the calculated light-scattering kinetic curves (*thin line*) for the two models for the case that excess S1 is mixed with actin in the absence of Ca^{++} are compared with the pyrene fluorescence kinetic curves.

Predictions of the Hill Model

Fitting the binding isotherm

To assign the kinetic rate constants of the Hill model, we first need to assign the equilibrium constants and the cooperativity parameters of the model: K_1, K_2, L', and Y. These parameters can be obtained by fitting the model to the experimental binding isotherms shown in Fig. 2, *A* and *B* of McKillop and Geeves (1993). Because the experimental binding data has been fit with the Geeves model (Table 1 of McKillop and Geeves, 1993), we derived the equilibrium constants by fitting the Hill model to Eq. 16 using the equilibrium constants listed in Table 1 of McKillop and Geeves (1993). The results are shown in Table 2. As one can see, the Hill model can fit the binding data of McKillop and Geeves with several sets of parameters. In general, the binding isotherm predicted by the Hill model is insensitive to K_1. In contrast, K_2, L', and Y are limited to a small range of values. It is also found that the values of Y in the presence and absence of Ca^{++} are close to 1.

One must note that the values of L' and Y obtained here are quite different from those obtained by Hill et al. (1980) and by Williams and Greene (1983). In general, the L' evaluated here using the data of McKillop and Geeves is about 5–10 times larger than those obtained by others. In contrast, the value of Y is about 4–20 times smaller. These discrepancies may come from different methods used in measuring the binding isotherms.

TABLE 1 Kinetic rate constants of the Geeves model

	$+Ca^{++}$	$-Ca^{++}$
α_B	10000.0	30.0
α_{-B}	100.0	100.0
α_T	90.0	39.0
α_{-T}	3000.0	3000.0
k_{+1}	2.6	2.6
k_{-1}	20.0	20.0
k_{+2}	4820.0	3760.0
k_{-2}	20.0	20.0

k_{+1} has units of $\mu M^{-1}s^{-1}$; other rate constants have units of s^{-1}.

Fitting the family of time courses of S1 binding to actin

As discussed before, there are six independent rate parameters for the Hill model. However, as shown in Table 2, the binding isotherm is insensitive to the value of K_1. Therefore, K_1 is also considered as an independent parameter in this case. Thus, there are a total of seven independent parameters to be determined in the modeling. One must note that Y_1 and Y_2 in Eqs. 13 and 14 are not independent parameters, because they can be evaluated from Eqs. 5 and 6 when the values of Y, α_0, and β_0 are assigned.

After the values of the independent parameters are chosen, the kinetics of S1 binding is evaluated by Monte Carlo simulation. A set of parameters found to fit the calculated kinetic curves of the Geeves model at the three conditions in Fig. 4 is listed in Table 3. The simulated curves are shown as solid lines in Fig. 4 together with the results of the Geeves model simulation. As one can see from the figures, the kinetic curves calculated for the Hill model using the parameters in Table 3 are almost identical with those calculated for the Geeves model for the case where [S1] $\geq$ [actin]. Most importantly, the Hill model is also able to generate the lag. In the case where [actin] $>$ [S1], the Hill model predicts a slightly slower binding curve in the absence of Ca^{++}. However, this difference is too small to permit experimental discrimination between the two models.

DISCUSSION

The three- and two-state kinetic models generate similar time courses of S1 binding to regulated actin

As shown in Fig. 4, *A–C*, the two-state Hill model and the three-state Geeves model give very similar predictions for

TABLE 2 Equilibrium constants obtained by fitting the Geeves' equilibrium binding data to the Hill model

		Hill model				
	Geeves Model	K_1	K_2	Y	L'	RMSD
$+Ca^{++}$	$K_1^G = 0.13$	0.001	31.45	0.9722	33.75	1.0
	$K_2^G = 241$	0.01	31.45	0.9742	33.75	1.0
	$K_T = 0.03$	0.05	31.46	0.9828	33.72	1.0
	$K_B = 100$	0.1	31.46	0.9937	33.69	1.0
		0.2	31.46	1.016	33.62	1.0
		1	31.50	1.210	32.91	1.0
		10	31.46	1.093	16.91	0.9989
$-Ca^{++}$	$K_1^G = 0.13$	0.001	24.57	0.9857	334.6	1.0
	$K_2^G = 188$	0.01	24.57	0.9914	334.2	1.0
	$K_T = 0.013$	0.05	24.57	1.008	332.4	1.0
	$K_B = 0.3$	0.1	24.58	1.030	330.3	1.0
		0.2	24.58	1.074	325.8	1.0
		1	24.63	1.497	288.0	0.99991
		2	24.65	2.263	238.7	0.9995
		10	24.19	66.98	29.97	0.98

The fitting was carried out using SigmaPlot.
RMSD, root-mean-square-deviation.
K_1, K_2, and K_1^G are in units of μM^{-1}. The others are unit-less.

the change in pyrene actin fluorescence upon the binding of S1. In the presence of Ca^{++}, the time course can be expressed by a one-exponential function at both high and low S1. Second, in the absence of Ca^{++}, the one-exponential kinetic behavior is generated only in the low S1 case. At high S1, the rate of fluorescence change is slow at the beginning of the reaction, forming a lag that precedes the rapid exponential phase. After the lag phase, the fluorescence increases exponentially. Third, when actin is in excess of S1, the rate of S1 binding is higher in the presence of Ca^{++} than in the absence of Ca^{++}. The ratio of the apparent rate constants of the two curves is found to be ~4, similar to that found experimentally. The Hill model differs slightly from the Geeves model only in the high actin case in the absence of Ca^{++}. Even under this condition, the difference is too small to allow distinction between the two models. The results shown here imply that the two models can be considered as kinetically equivalent in regards to the time course of S1 binding to regulated actin.

TABLE 3 Parameters of the Hill model used to fit the kinetic curves in Fig. 4 calculated for the Geeves model

	$+Ca^{++}$	$-Ca^{++}$
α_0	200.0	200.0
β_0	300.0	300.0
Y_1	4.682	15.27
Y_2	0.208	0.0703
k_1	5.0	0.6
k_1'	500.0	3.0
k_2	2.831	2.212
k_2'	0.09	0.09
γ	0.8	0.8
δ	0.5	0.5

α_0, β_0, k_1', and k_2' are in units of s^{-1}; k_1 and k_2 are in units of $\mu M^{-1}s^{-1}$; The rest are dimensionless.

Mechanism of generation of the lag in the Hill model

The most important finding of this modeling work is the fact that the Hill model can generate the experimentally observed lag in the time course of S1 binding to regulated actin when an excess of S1 is mixed with actin in the absence of Ca^{++}. The generation of this lag by the Hill model depends on the kinetic parameters of the model in a complicated way. Here, we present a qualitative but general explanation of why the lag is present only in the case when Ca^{++} is absent and S1 is in excess of actin and not in other experimental conditions.

In general, to generate a lag in the time course of pyrene fluorescence, S1 must remain unbound or bound in state 1 for some time before turning into state 2 at early times of the binding reaction. For example, if the reactions along the upper path (binding of S1 to actins in state 1) are slower than those in the lower path, then systems taking the binding route, *path B* in Fig. 5, will have a better chance of generating a lag than those taking path A. This is exactly the reason for the Hill model to generate the lag with the parameters in Table 3. At first, let us discuss the high S1 case. In Fig. 6, the net transition flux (forward minus backward) of each reaction step (S1 binding or transition between states 1 and 2) for a Tm–Tn–actin unit, as evaluated from the Monte Carlo simulation, is shown as a function of time. As shown in Fig. 6 *A*, there are only four significant net fluxes with transitions starting from state 1 for the $+Ca^{++}$ case, $J_{10\to11}$, $J_{11\to21}$, $J_{11\to12}$, and $J_{12\to22}$

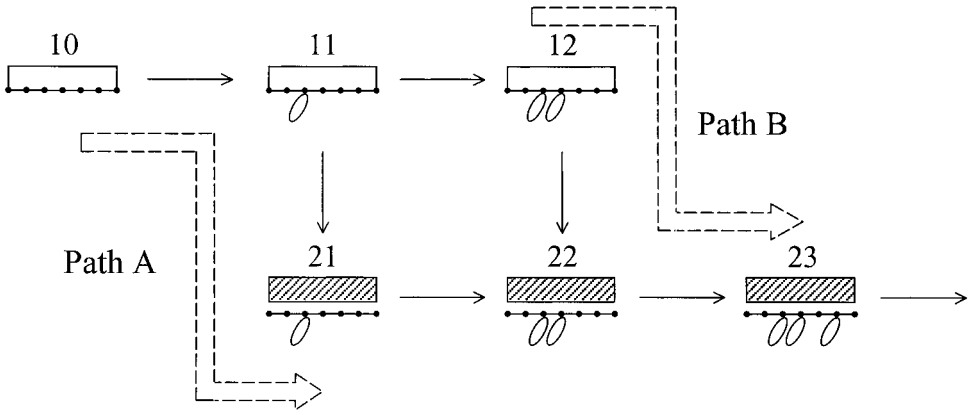

FIGURE 5 Possible binding pathways for the binding of S1 to a Tm–Tn–actin unit at the early times of the binding reaction. In path *A*, a unit with one bound S1 changes from state 1 to state 2 before binding another S1. In path *B*, the transition from state 1 to state 2 does not occur appreciably until the unit binds with two S1. Path *B* would produce a lag in the kinetic curve of pyrene-fluorescence and light scattering if the rate constant of binding S1 to actin in state 1 (those in the upper line) is smaller than that of binding to state 2.

where $in \rightarrow jm$ represents the transition from a unit in state i with n bound S1 to a state in j with m bound S1. The fact that $J_{10\rightarrow11}$ and $J_{11\rightarrow21}$ are almost identical and that they are much larger than $J_{11\rightarrow12}$ and $J_{12\rightarrow22}$ (specifically, $J_{11\rightarrow21} > J_{11\rightarrow12}$) implies that the main pathway of the S1 binding of the system is $10\rightarrow11\rightarrow21\rightarrow22\rightarrow\cdots$ (*path A* in Fig. 5). In contrast, for the $-Ca^{++}$ case $J_{11\rightarrow12}$ is much larger than $J_{11\rightarrow21}$, as shown in Fig. 6 *B*. As a result, *path B* ($10\rightarrow11\rightarrow12\rightarrow22\rightarrow\cdots$) is the dominant pathway in this case. The flux curves in Fig. 6, *C* and *D* are consistent with the proposed pathways. For example, as one can see in Fig. 6 *C*, $J_{21\rightarrow22}$ is the largest flux at the early times for the $+Ca^{++}$ case, indicating that all the subsequent S1 binding in state 2 derives from the $11\rightarrow21$ transition (*path A*). In

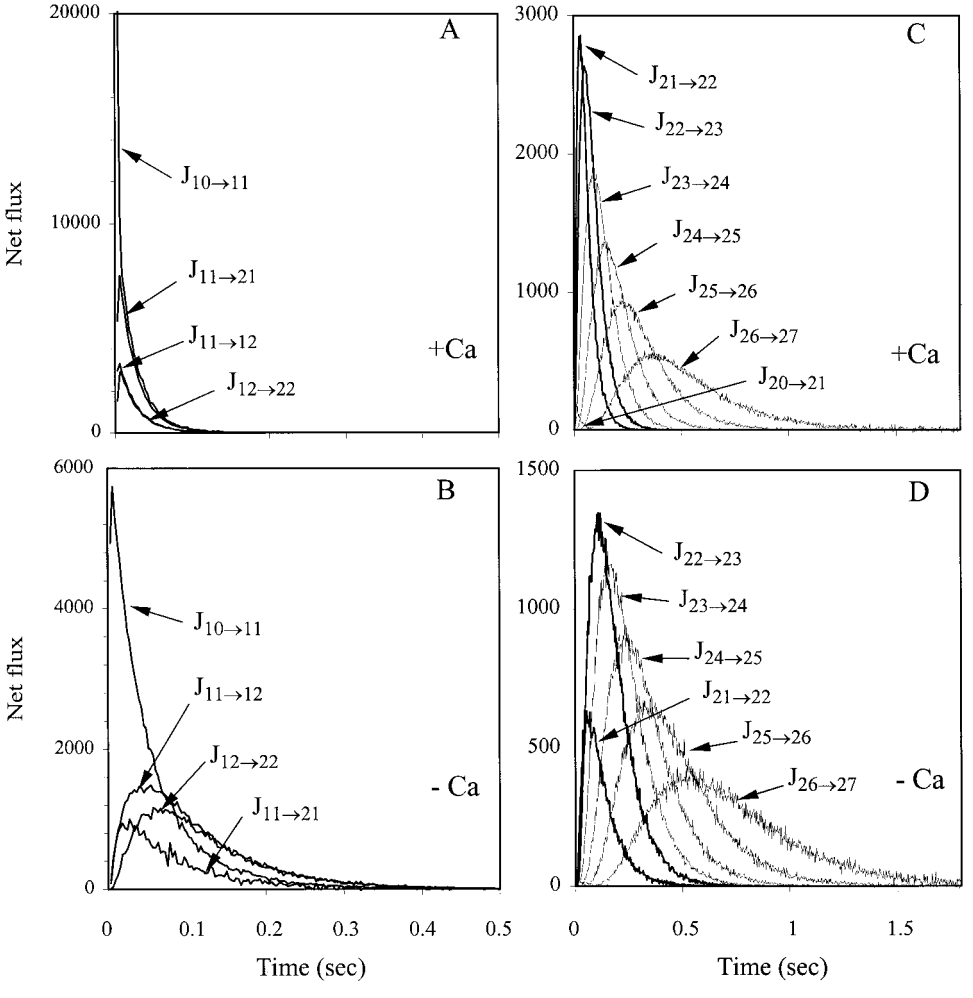

FIGURE 6 Net fluxes of some transition steps in the Hill model evaluated using the parameters in Table 3 for the high [S1] case: $c^0_{S1} = 2.5$ μM and $c^0_A = 0.5$ μM. The first symbols, i and j, in $J_{in\rightarrow jm}$ represent the state of the unit, and the second symbols, n and m, represent the number of bound S1. For example, $11\rightarrow21$ represents the transition of a Tm–Tn–actin unit with one bound S1 from state 1 to state 2, etc. Net fluxes evaluated for the case with Ca^{++} present are shown in panels *A* and *C*; those with Ca^{++} absent are shown in panel *B* and *D*.

contrast, the fact that $J_{22\rightarrow23}$ is much larger than $J_{21\rightarrow22}$ at early times for the $-Ca^{++}$ case means that the supply of $J_{22\rightarrow23}$ mainly comes from $J_{12\rightarrow22}$ (*path B*).

When the concentration of actin is much larger than S1 (the low S1 case), the number of S1 bound to a Tm–Tn unit in state 1 at early times of the reaction will be at most one, in both $+Ca^{++}$ and $-Ca^{++}$. That is, the probability of binding two or more S1 to a Tm–Tn–actin unit is very low in both cases. As a result, path A is the dominant pathway and no lag is expected.

It is important to point out that, as shown in Fig. 5, the S1 binding in the two-state Hill model involves many binding steps and many biochemical states, not just two as the word "two-state" implies. This is exactly why the model is able to generate the lag in the kinetic binding curve. There are even more states and more reaction steps in the Hill model if the binding of Ca^{++} is treated explicitly. In this case, modeling the lag in the kinetics of S1 binding is expected to be much easier.

Lag also occurs in light scattering

In this study, we were mainly concerned with the kinetic curves of pyrene fluorescence that measures the time course of S1-bound actin in the on state only, because this is the quantity measured by McKillop and Geeves (1993). As shown by Trybus and Taylor (1980), the lag was also found in the light scattering kinetic curve, which measures the total S1-bound actin in both on and off states as a function of time. The kinetics of light scattering can be easily calculated using the formalisms developed here. To see whether the light scattering could be used for model differentiation, we also carried out light-scattering calculations for the three cases in Fig. 4 using the same sets of parameters in Tables 1 and 3. We found that both models produced almost identical light-scattering kinetic curves (data not shown). A lag was also found for the case when excess S1 is mixed with actin in the absence of Ca^{++} for both models. However, the lag in light scattering is smaller (less sharper) than that in pyrene fluorescence (see the inset in Fig. 4 *A*). Why the Hill model is able to generate a smaller lag in light scattering in this excess-S1–no-Ca case can be explained also using the same arguments presented above for pyrene fluorescence. That is, processes taking path B in Fig. 5 are also expected to generate lags in light scattering, but not those taking path A. The reason for this is that the rate of binding of S1 to actin in state 1 (*upper line* in Fig. 5) is much slower than that in state 2 (*lower line* in Fig. 5), because $k_1 < k_2$ as shown in Table 3. Thus, although the binding of S1 to actin in state 1 also contributes to the light scattering signal, the time course of the signal is very different at early and late times, if the process takes path B: slow at first and fast later, thus forming a lag. The lag in light scattering is smaller than in pyrene fluorescence, because binding reactions of S1 to actin in state 1 in the upper line of Fig. 5 also contribute to the light scattering signal; in pyrene fluorescence, those reactions are completely silent.

Ca^{++} effects on observed rate constants

In fitting the Hill model to the kinetic curves generated by the Geeves model in Fig. 4, some of the parameters for the Hill model had to be Ca^{++} dependent. Specifically, the rate constants for attachment and detachment of S1 to actin in state 1 (the off state) have to be quite different in the presence and absence of Ca^{++}, unlike those in the Geeves model (see Tables 1 and 3). There is experimental evidence for Ca^{++}-dependence of cross-bridge binding, at least in the presence of nucleotides. In the presence of ATPgS, the affinity of S1 to regulated actin is not significantly affected by Ca^{++} (Resetar and Chalovich, 1995). However, the rate of cross-bridge detachment, in single-muscle fiber preparations, is decreased in the presence of Ca^{++} (Kraft et al., 1992). The simulations done here were for the case where no nucleotide was present, so a direct comparison with experimental data is impossible. However, this Ca^{++}-dependence of the kinetics of binding may be a useful experimental approach to testing models of regulation. It will be particularly important in future studies to have accurate and independent determinations of the values of L' and Y under the conditions used for kinetic measurements.

Potential value of the Hill model

We have shown here that the Hill model is not at a disadvantage from other models in terms of describing the time course of binding. Recently, we have shown that the Hill model was able to simulate the activation kinetics of actin filaments in single fiber experiments (Brenner and Chalovich, 1999). Also, there are a sufficient number of physical states to accommodate the known structural changes of the regulated actin filament. The natural question is whether the Hill model has any advantages that would justify its continued study. The Hill model has been shown to predict the steady-state kinetics of ATP hydrolysis under a variety of conditions (Hill et al., 1981). The Geeves model describes the effects of Ca^{++} on the binding of myosin to actin but does not include changes in the rates of other transitions that might occur with changes in Ca^{++}. Therefore, the ability of this model to predict steady-state kinetics of ATP hydrolysis cannot be rigorously examined. In the Geeves model, there is a significant change in the affinity of the S1–ATP state for binding to actin in the presence and absence of Ca^{++} (McKillop and Geeves, 1993). This occurs because of a $>$4-fold change in the distribution of the closed state relative to the blocked state in the presence of Ca^{++}. However, the actual difference in affinity of S1 for regulated actin during steady-state ATP hydrolysis between the high and low Ca^{++} conditions is two-fold or less (Chalovich et al.,

1981; Chalovich and Eisenberg, 1982; Wagner and Giniger, 1981). Experiments done in single-muscle fibers also indicate that there is little effect of Ca^{++} on the binding affinity of myosin to actin in the presence of ATP (Kraft et al., 1992). The Geeves model could be consistent with these findings if the state formed between myosin and actin in the presence of ATP were a collision intermediate. However, it is hard to imagine how a collision intermediate could produce a measurable stiffness in muscle fiber experiments.

In agreement with the small Ca^{++} effect on S1–ATP binding, there is only a small change in the K_M for actin activated ATP hydrolysis, but a large change in the k_{cat} with Ca^{++} (Chalovich and Eisenberg, 1982). The Geeves model could accommodate a large change in k_{cat} by including additional regulated steps that are not present in the current model. However, the >4-fold change in the distribution between the blocked and closed states upon increasing the Ca^{++} concentration would appear to result in a larger change in the K_M than has been observed for S1 binding. Note that a change of 4–5-fold would be consistent with some experiments with HMM but present models are based on experiments done with S1 (Chalovich, 1992 and references therein). In the Hill model, it is possible to obtain rates of ATPase activity for regulated actin that exceed those of pure actin as observed in some situations. Such potentiation in ATPase rates was reported by Eisenberg and Kielley (1970). Bremel et al. (1972) reported more than a doubling of the ATPase rate for regulated actin over pure actin at low ATP concentrations or at very high S1 concentrations. More recently, it was shown that changes in the type of troponin T in the troponin complex can result in an enhanced rate even at normal concentrations of ATP and at low S1 concentrations (Fredricksen and Chalovich, 2001).

CONCLUSIONS

1. Mathematical procedures for the evaluation of kinetics of S1 binding to regulated actin filaments have been developed for both the two-state Hill model and the three-state Geeves model. These procedures are useful for the determination of the basic rate constants of the binding processes for both models when the kinetic curves of S1 binding are measured.
2. The two models yield qualitatively similar simulations of the time course of S1 binding to regulated actin measured using fluorescent pyrene-labeled actin. Specifically, the two-state Hill model can also generate the lag observed in the time course of S1 binding when excess S1 is mixed with actin in the absence of Ca^{++}. As far as fitting the entire time-dependent kinetic curve of S1 binding to regulated actin filament is concerned, there is no difference between the Hill model and the Geeves model. Thus, the two-state model cannot be excluded based on equilibrium and pre-steady-state kinetics of S1 binding to regulated actin.
3. Using the same sets of kinetic parameters in Tables 1 and 3, we found that the Hill and the Geeves models also yielded similar light-scattering kinetics. Specifically, a lag was also found in the time course of light scattering when mixing excess S1 with actin in the absence of Ca^{++}. Thus, light scattering kinetic curves also are not very useful in the differentiation of the two models.
4. The results obtained in this study indicate that the activation of regulated actin from the off to the on state in the absence of Ca^{++} may not require the existence of an intermediate state as required by the Geeves model. However, it is important to note that neither model has been rigorously tested for the ability to simulate multiple sets of experimental data.

The analyses presented in this paper are based on the equilibrium and kinetic data of McKillop and Geeves (1993) measured for nucleotide-free S1. The equilibrium constants derived for the Hill model using their data are greatly in discrepancy with those obtained by others (Hill et al., 1980; Williams and Greene, 1983). Whether the Hill and the Geeves models actually can or cannot be differentiated based on equilibrium and kinetic measurements of S1 binding may require matched and accurately measured equilibrium and kinetic binding curves of S1 with different bound nucleotides.

APPENDIX: EFFECT OF COOPERATIVITY ON TRANSITION RATE CONSTANTS BETWEEN STATES 1 AND 2

In this Appendix, Eqs. 13 and 14 will be derived based on the Transition Rate Theory of Eyring (Chang, 1981). According to this theory, transition rate constants, α_m and β_m, between states 1 and 2 in the absence of nearest-neighbor interactions (cooperativity) can be expressed as

$$\alpha_m = k \exp(-(E^{\neq} - E_1)/k_B T), \quad \text{(A1)}$$

$$\beta_m = k \exp(-(E^{\neq} - E_2)/k_B T), \quad \text{(A2)}$$

where k is a constant, E_1 and E_2 are the free energies of an isolated unit in states 1 and 2, respectively, and $E^{\neq}$ is the free energy of the activated transition state of the reaction, as shown in Fig. 7. The factor $k_B T$ is the product of the Boltzmann constant and the temperature. In the presence of cooperativity, the energy profile of the reaction is altered. As shown in Fig. 7, let ΔE_1, ΔE_2, and $\Delta E^{\neq}$ represent the change of free energies of state 1, state 2, and the activated state, respectively. Then, the new rate constants $\bar{\alpha}_m$ and $\bar{\beta}_m$ can be obtained as

$$\bar{\alpha}_m = k \exp(-(E^{\neq} + \Delta E^{\neq} - E_1 - \Delta E_1)/k_B T) = \alpha_m \exp(-(\Delta E^{\neq} - \Delta E_1)/k_B T), \quad \text{(A3)}$$

$$\bar{\beta}_m = k \exp(-(E^{\neq} + \Delta E^{\neq} - E_2 - \Delta E_2)/k_B T) = \beta_m \exp(-(\Delta E^{\neq} - \Delta E_2)/k_B T), \quad \text{(A4)}$$

where Eqs. A1 and A2 have been used to obtain the second equality in both Eqs. A3 and A4. Now, let N_1 be the number of the two neighboring units

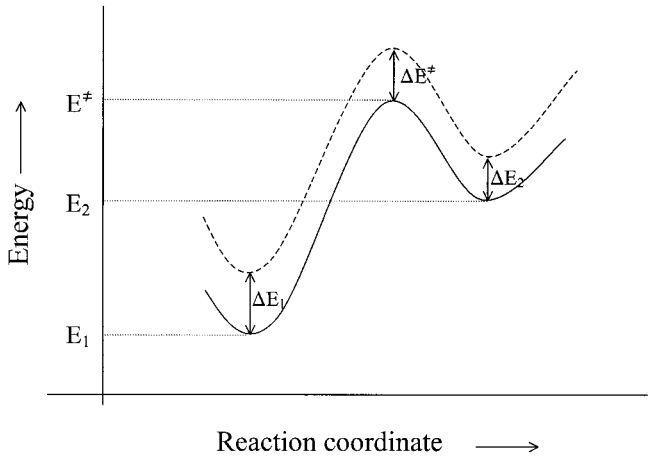

FIGURE 7 Schematic free energy profile for the reaction between state 1 and state 2 of an isolated Tm–Tn–actin unit (*solid line*) and a unit with nearest-neighbor interactions (*dashed line*). The free energy profiles are assumed to be unaffected by the number of S1 bound to the unit. The magnitudes of ΔE_1 and ΔE_2 depend on the number of neighbors in state 1 and the unit–unit interaction between two neighboring actin units (see Eqs. A5 and A6). $\Delta E^{\neq}$ is defined in Eq. A7.

(on the two sides of the unit undergoing the transition) that are in state 1. Then, we have

$$\Delta E_1 = N_1 w_{11} + (2 - N_1) w_{12}, \tag{A5}$$

$$\Delta E_2 = N_1 w_{12} + (2 - N_1) w_{22}, \tag{A6}$$

where w_{ij} is the nearest-neighbor interaction energy as shown in Fig. 1 *A*. Let us assume that $\Delta E^{\neq}$ can be expressed as a linear combination of ΔE_1 and ΔE_2,

$$\Delta E^{\neq} = \delta \Delta E_1 + (1 - \delta) \Delta E_2, \tag{A7}$$

where δ is a constant valued between 0 and 1. Then, it is easy to show that Eqs. 13 and 14 can be obtained after substituting Eqs. A5–A7 into Eqs. A3 and A4 and using the identities

$$Y_1 = Y_{11}/Y_{12} \equiv \exp(-(w_{11} - w_{12})/k_B T),$$

$$Y_2 = Y_{22}/Y_{12} \equiv \exp(-(w_{22} - w_{12})/k_B T).$$

REFERENCES

Brenner, B., and J. M. Chalovich. 1999. Kinetics of thin filament activation probed by fluorescence of *N*-((2-(iodoacetoxy)ethyl)-*N*-methyl)amino-7-nitrobenz-2-oxa-1,3-diazole-labeled troponin I incorporated into skinned fibers of rabbit psoas muscle: implications for regulation of muscle contraction. *Biophys. J.* 77:2692–2708.

Bremel, R. D., J. M. Murray, and A. Weber. 1972. Manifestations of cooperative behavior in the regulated actin filament during actin-activated ATP hydrolysis in the presence of calcium. *Cold Spring Harbor Symp. Quant. Biol.* 37:267–275.

Chalovich, J. M., P. B. Chock, and E. Eisenberg. 1981. Mechanism of action of troponin–tropomyosin. Inhibition of actomyosin ATPase activity without inhibition of myosin binding to actin. *J. Biol. Chem.* 256:575–578.

Chalovich, J. M., and E. Eisenberg. 1982. Inhibition of actomyosin ATPase activity by troponin–tropomyosin without blocking the binding of myosin to actin. *J. Biol. Chem.* 257:2432–2437.

Chalovich, J. M. 1992. Actin mediated regulation of muscle contraction. *Pharmacol. Ther.* 55:95–148.

Chalovich, J. M., Y.-d. Chen, R. Dudek, and H. Luo. 1995. Kinetics of binding of caldesmon to actin. *J. Biol. Chem.* 270:9911–9916.

Chang, R. 1981. Physical Chemistry with Applications to Biological Systems. Macmillan Publishing Co., Inc., New York, N.Y. 371–374.

Chen, Y.-d., and T. L. Hill. 1983. Use of Monte Carlo calculations in the study of microtubule subunit kinetics. *Proc. Natl. Acad. Sci. U.S.A.* 80:7520–7523.

Eisenberg, E., and W. W. Kielley. 1970. Native tropomyosin: effect on the interaction of actin with heavy meromyosin and subfragment 1. *Biochem. Biophys. Res. Comm.* 40:50–56.

Fredricksen, R. S., and J. M. Chalovich. 2001. Potentiation of actin activated ATPase activity by a hybrid troponin. *Biophys. J.* 80:342a.

Geeves, M. A., and D. J. Halsall. 1987. Two-step ligand binding and cooperativity. A model to describe the cooperative binding of myosin subfragment 1 to regulated actin. *Biophys. J.* 52:215–220. [published erratum in *Biophys. J.* 53:845, 1988].

Greene, L. E., and E. Eisenberg. 1980. Cooperative binding of myosin subfragment-1 to the actin–troponin–tropomyosin complex. *Proc. Natl. Acad. Sci. U.S.A.* 77:2616–2620.

Hill, T. L., E. Eisenberg, and L. Greene. 1980. Theoretical model for the cooperative equilibrium binding of myosin subfragment 1 to the actin–troponin–tropomyosin complex. *Proc. Natl. Acad. Sci. U.S.A.* 77:3186–3190.

Hill, T. L., E. Eisenberg, and J. M. Chalovich. 1981. Theoretical models for cooperative steady-state ATPase activity of myosin subfragment-1 on regulated actin. *Biophys. J.* 35:99–112.

Kraft, T., L. C. Yu, H. J. Kuhn, and B. Brenner. 1992. Effect of Ca^{2+} on weak cross-bridge interaction with actin in the presence of adenosine 5′-[γ-thio]triphosphate. *Proc. Natl. Acad. Sci. U.S.A.* 89:11362–11366.

McKillop, D. F., and M. A. Geeves. 1991. Regulation of the acto.myosin subfragment 1 interaction by troponin/tropomyosin. Evidence for control of a specific isomerization between two acto.myosin subfragment 1 states. *Biochem. J.* 279:711–718.

McKillop, D. F., and M. A. Geeves. 1993. Regulation of the interaction between actin and myosin subfragment 1: evidence for three states of the thin filament. *Biophys. J.* 65:693–701.

Resetar, A. M., and J. M. Chalovich. 1995. Adenosine 5′-(γ-thiotriphosphate): an ATP analog that should be used with caution in muscle contraction studies. *Biochemistry.* 34:16039–16045.

Tobacman, L. S., and C. A. Butters. 2000. A new model of cooperative myosin–thin filament binding. *J. Biol. Chem.* 275:27587–27593.

Trybus, K. M., and E. W. Taylor. 1980. Kinetic studies of the cooperative binding of subfragment 1 to regulated actin. *Proc. Natl. Acad. Sci. U.S.A.* 77:7209–7213.

Vibert, P., R. Craig, and W. Lehman. 1997. Steric-model for activation of muscle thin filaments. *J. Mol. Biol.* 266:8–14.

Wagner, P. D., and E. Giniger. 1981. Calcium-sensitive binding of heavy meromyosin to regulated actin in the presence of ATP. *J. Biol. Chem.* 256:12647–12650.

Williams, D. L., Jr., and L. E. Greene. 1983. Comparison of the effects of tropomyosin and troponin-tropomyosin on the binding of myosin subfragment 1 to actin. *Biochemistry* 22:2770–2774.

Williams, D. L., Jr., L. E. Greene, and E. Eisenberg. 1988. Cooperative turning on of myosin subfragment 1 adenosine triphosphatase activity by the troponin–tropomyosin–actin complex. *Biochemistry.* 27:6897–6993.

Xu, C., R. Craig, L. Tobacman, R. Horowitz, and W. Lehman. 1999. Tropomyosin positions in regulated thin filaments revealed by cryoelectron microscopy. *Biophys. J.* 77:985–992.

Zou, G., and G. N. Phillips, Jr. 1994. A cellular automaton model for the regulatory behavior of muscle thin filaments. *Biophys. J.* 67:11–28.